Brain Image Registration Based on Curve Mapping

Chris Davatzikos and Jerry L. Prince

Department of Electrical and Computer Engineering
Johns Hopkins University
Baltimore, MD 21218
e-mail: hristos@mashie.ece.jhu.edu and prince@mashie.ece.jhu.edu

Abstract

A new two-stage approach for brain image registration is proposed. In the first stage, an active contour algorithm is used to establish a length-preserving, one-to-one mapping between the cortical and the ventricular boundaries in the two images to be registered. This mapping is used in the second step by a two-dimensional transformation which is based on an elastic body deformation. This method was tested by registering magnetic resonance images to both photographic pathology images and atlas images.

I. Introduction

Registration of both intra-subject and inter-subject images has been the subject of extensive study in the medical imaging literature. It is important for several reasons. First, images obtained through different modalities can be properly superposed only after accurate registration. Visualization and quantitative analysis can be improved by such superposition. Second, atlas images accurately registered to patient data can be used for automatic identification of brain anatomy and for lesion localization. Third, image registration can assist in monitoring treatment by, for example, allowing accurate comparison of brain tumor size and position during treatment over time. Finally, it is hypothesized that proper statistical study of the morphology of both normal and diseased brains can be conducted only with good registration across diverse populations. This research contributes to the field of automated brain image registration by introducing the use of a length-preserving active contour algorithm and a new nonlinear registration algorithm.

Various techniques for image registration have been proposed, each having its own advantages and disadvantages, which are briefly summarized in Section II. The approach we propose in this paper has two main advantages over existing registration methods: it can describe large, nonlinear deformations, and it requires minimal human intervention. In our approach, we decompose the registration problem into two steps. In the first step, we apply an active contour algorithm [1] to each of the two images to be registered in order to obtain a one-to-one mapping between a set of curves that sit on the boundaries of brain regions, which can be segmented based on their intensity values. In the second step, we use this point-to-point correspondence to obtain a full 2-D transformation, allowing either image to be geometrically warped into correspondence with the other. Gray-scale information is only required by the active contour algorithm, so our registration approach is not based on image similarity measures.

The 2-D transformation we propose for the second step is termed the *elastic deformation transformation* or EDT. It is based on the premise that the geometric deformation between the two brains is adequately described as a rigid body motion followed by an elastic deformation. EDT describes a large class of deformations and can easily accommodate manually defined landmark points. Moreover, because the images are modeled as elastic sheets, they maintain their major geometric features after the warping procedure, which is a desired characteristic for the application considered in this paper, since the brains of different individuals tend to have a similar gross structure.

II. Registration Algorithms

Let $I_1(\mathbf{x}) = I_1(x, y)$ and $I_2(\mathbf{u}) = I_2(u, v)$ be the image intensity functions of a pair of images to be registered. Here, $\mathbf{x} = (x, y)$ and $\mathbf{u} = (u, v)$ denote pixel coordinates in the image domains $\mathcal{D}_1$ and $\mathcal{D}_2$, respectively, which we take to be the rectangular image frames (expanded if necessary to accommodate an expansion of one domain into the other). Image registration is defined as the problem of finding a transformation $\mathbf{U}(\mathbf{x}) = (U(x, y), V(x, y))$ that maps $\mathcal{D}_1$ into $\mathcal{D}_2$, so that the resulting image $I_3(\mathbf{U}(\mathbf{x}))$ is in *geometric correspondence* with $I_2(\mathbf{u})$. We note that the actual image values corresponding to registered coordinates need not be similar. The various image reg-

0-8186-5802-9/94 $3.00

istration techniques that have been proposed in the literature can be classified into three major categories — polynomial transformations, similarity-based methods, and boundary-based methods— as briefly described in the remainder of this section.

A. Polynomial Transformation Methods

Polynomial transformations are based on the assumption that the that brings $\mathcal{D}_1$ and $\mathcal{D}_2$ into geometric correspondence is sufficiently described by a polynomial of degree n. The coefficients of this polynomial are computed using linear regression, if at least $\frac{1}{2}(n+1)(n+2)$ landmark points are defined in the two images. Although any transformation can be described by a polynomial through a Taylor series expansion, in practice the numerical instabilities that are typically present in higher degree polynomial interpolation and the requirement for many landmark points – usually manually provided – limit these methods to the use of low degree polynomials.

In particular, the most popular technique in this class of methods is the linear transformation [2, 3, 4, 5]. In general, linear transformation methods can provide accurate registration only under the assumption that the objects appearing in $I_1(\cdot)$ and $I_2(\cdot)$ differ only by a rotation, translation, and scaling in both axes. This is true in intra-subject registration problems; but in inter-subject registration problems, highly nonlinear deformations are usually present. An example of this is the registration of atlas images to scanned images, an important problem in brain-mapping applications.

Piecewise polynomial transformations have also been proposed. In particular, Bookstein describes a spline interpolation approach for registering two brain images from a set of landmark pairs [6]. Although spline interpolation methods avoid, in general, the problem of non-realistic oscillations caused by polynomial interpolation, they also depend on the availability of a large set of landmark points.

B. Similarity-Based Methods

These methods use the similarity between two images as a criterion for correct registration. In [7, 8] an elastic deformation, based on the cross-correlation coefficient between the images, is iteratively applied to one of the images until it matches the other. This method assumes that a rough initial registration is provided and the two images are very similar to each other. Since this assumption is not always satisfied in practice, this approach can yield false matches that correspond to local minima of the energy function defined in [7].

A new similarity technique has been proposed recently by Miller et al. [9]. This method assumes a known map between the image intensities (assuming correct registration) and allows for a visco-elastic deformation in a probabilistic formulation. Although this approach is promising, it currently has two main limitations. First, there is typically no known intensity correspondence between different imaging modalities; and second, because of heavy computational demands, acceptable solutions are found only when the deformation is very small.

C. Boundary-Based Methods

Boundary-based methods use information about the registration of object boundaries in order to derive a full 2-D registration. Moshfeghi has proposed a method based on an iterative deformation of boundaries [10]. This method is computationally very expensive and is very sensitive to errors in the initial registration of the objects. Specifically, if a small rotational error is introduced during the initialization of the algorithm, the contour of the first image will deform towards the wrong configuration, and this error will propagate to the remaining image points.

Methods based on boundary registration have also been formulated in three dimensions, but are mostly based on rigid body transformations. Pelizzari et al. [11] developed a popular method based on an iterative search in the parametric space. Thirion et al. [12] proposed a similar technique based on matching points of high curvature on the skull. Approaches based on rigid body motion are valid only for same-patient imaging, but are not generally applicable to atlas matching.

III. Nonlinear Registration Using an Active Contour Algorithm

In this section we present a new two-step approach to image registration. The first step creates a one-to-one mapping between a set of curves that can be identified in the two images to be registered using an active contour algorithm which is described below (although the only type of images that we consider in this paper is brain images, our approach applies to other problems also). The boundary of the brain constitutes an example of a curve that we commonly identify in brain images. A fundamental assumption required by this step is that the curves that are identified in one of the images can be transformed into their corresponding curves in the other image by uniformly scaling their length and bending them like a string into conformation. If they must be locally stretched in order to conform, then our approach is not valid. A simple modification, however, in which manually provided (or otherwise detected) points of correspondence on these curves are given can be made to allow nonuniform curve scaling.

The second step in our registration algorithm uses the point-to-point curve correspondence established in the first step to prescribe a transformation for each point in the image domain. Specifically, we deform the images elastically under the presence of external forces that are defined on the sets of curves identified in the images. The magnitude of these forces becomes zero when the curve-to-curve correspondences obtained through our active contour algorithm in the first step are satisfied. We begin this section by reviewing the active contour algorithm.

A. Active Contour Algorithm

In [1] we presented an algorithm that reconstructs the spine of uniform thickness ribbons (see also [13, 14, 15]). This reconstruction comprises a map from the unit interval to the spine that is nearly isometric — that is, length-preserving — up to a single length scaling factor. In brain image analysis, we use ribbons to model the cortical cross-sections (which have a fairly uniform thickness), and boundaries of brain regions (which have infinitesimal thickness). Since our active contour algorithm is used directly in step one, we give a brief overview and discussion of its key properties.

Active contours were introduced in [16], and since then they have been extensively in image analysis and computer vision. An active contour is an elastic curve that deforms under the presence of internal and external forces. The internal forces maintain its connectivity and are responsible for its elastic behavior, while the external forces provide a mechanism for matching the elastic curve to the data. An active contour can be viewed as a set of $M+1$ points, with cartesian coordinates $\mathbf{x}_i = (x_i, y_i)$, $i = 0, ..., M$, connected to each other with springs, as shown in Fig. 1. The internal forces exerted on the point at $\mathbf{x}_i$ originate from the two springs that connect the point to its neighboring active contour points located at $\mathbf{x}_{i-1}$ and $\mathbf{x}_{i+1}$. The external force exerted on the point at $\mathbf{x}_i$ is an attractive force originating from a point $\mathbf{c}_i = \mathbf{c}(\mathbf{x}_i)$ within the ribbon (as in [1]). This point is located at the center of mass of the area defined by the intersection of the ribbon with a circular neighborhood around $\mathbf{x}_i$. Under the presence of these internal and external forces, the active contour undergoes a series of elastic deformations eventually balancing near the spine of the ribbon.

Our active contour algorithm finds a solution to the following set of nonlinear equations:

$$\mathbf{c}(\mathbf{x}_i) - \mathbf{x}_i + K_0 M^2 (\mathbf{x}_{i+1} + \mathbf{x}_{i-1} - 2\mathbf{x}_i) = 0\,,\ i = 1, ..., M-1\,, \tag{1}$$

subject to the boundary conditions

$$\mathbf{x}_0 = (\alpha, \gamma)\,,\ \mathbf{x}_M = (\beta, \delta). \tag{2}$$

These equations correspond to a force balance condition in which each active contour point $\mathbf{x}_i$ balances under the three forces described above. The following iterative algorithm is used to solve (1)

$$\mathbf{x}_i^{k+1} = \frac{\mathbf{c}(\mathbf{x}_i^k) + K_0 M^2 \left(\mathbf{x}_{i+1}^k + \mathbf{x}_{i-1}^k\right)}{2K_0 M^2 + 1}\,,\ i = 1, ..., M-1\,. \tag{3}$$

where superscripts give the iteration count.

It was shown in [1] that the $M-1$ equations in (1) are satisfied by the active contour that minimizes the energy function

$$\mathcal{E}(\mathbf{x}_0, ..., \mathbf{x}_M) = \mathcal{E}_F(\mathbf{x}_0, ..., \mathbf{x}_M) + K_0 \mathcal{E}_E(\mathbf{x}_0, ..., \mathbf{x}_M), \tag{4}$$

where

$$\mathcal{E}_F(\mathbf{x}_0, ..., \mathbf{x}_M) = \frac{1}{M} \sum_{i=0}^{M} P(\mathbf{x}_i)\,, \tag{5}$$

$$\mathcal{E}_E(\mathbf{x}_0, ..., \mathbf{x}_M) = M \sum_{i=0}^{M-1} \|\mathbf{x}_{i+1} - \mathbf{x}_i\|^2. \tag{6}$$

The function $P(\mathbf{x}_i)$ in (5) is a potential function which is zero if $\mathbf{x}_i$ belongs to the spine and rapidly increases as $\mathbf{x}_i$ moves away from the spine (see [1] for details).

B. Cortical and Ventricular Contour Extraction and Mapping

Given two images to be registered, our first step is to extract a set of curves sitting on the boundaries of a corresponding set of regions that can be segmented based on their intensity values. In this paper we will only consider the cortical and the ventricular boundaries. Each of these curves is mapped onto the unit interval using the active contour algorithm of the previous section. To do this, we first identify a set of boundary points for each of these brain regions, as indicated in the block diagram of Fig. 2. We use a two-dimensional region growing algorithm and one manually provided seed point for each of these brain regions. The points where the growing region terminates are the boundaries of each of these regions, and they are used as the "mass" by our active contour algorithm. We then initialize the active contour algorithm selecting the endpoints for each image and for each curve manually. The remaining points of the active contour are initialized at a circular configuration surrounding each region. Solving the equations in (1) for each image and for each curve separately yields a set of points $\mathbf{x}_0^k, \mathbf{x}_2^k, ..., \mathbf{x}_M^k$, $k = 1, ..., K$, which define K curves in the first image, and a set of points $\mathbf{u}_0^k, \mathbf{u}_2^k, ..., \mathbf{u}_M^k$ which define K curves in the second image. These points are nearly equidistantly distributed along the K curves in each image; therefore there exists a one-to-one isometric mapping of each curve to the unit interval. Consequently, there exists a one-to-one isometric mapping between the corresponding curves themselves. This mapping provides a correspondence between the point $\mathbf{x}_i^k$ of the k-th curve of the first image and the point $\mathbf{u}_i^k$ of the k-th curve of the second image, for $i = 0, ..., M$, and for $k = 1, \ldots, K$. This collection of landmark points is used in the transformations of the following two sections.

C. Elastic Deformation Transformation (EDT)

In this section we describe a new full two-dimensional transformation based on the active contour algorithm results. This method, which we call the *elastic deformation transformation* (EDT), assumes that the pixels in $\mathcal{D}_1$ are connected by springs. Those points in $\mathcal{D}_1$ that are part of

the K curves that were determined by the active contour algorithm have external forces encouraging them to deform to the coordinates of the corresponding points on the K curves in $\mathcal{D}_2$. EDT determines the elastic deformation caused by the combination of these external forces, the internal spring forces, and boundary conditions. If additional points of correspondence are provided, external forces are also exerted on those points.

Mathematically, EDT is based on the minimization of an energy function E, which we now define. Let $(x_{0,0}, y_{0,0})$ through $(x_{N,N}, y_{N,N})$ be the pixel locations in $\mathcal{D}_1$ and $(U_{0,0}, V_{0,0})$ through $(U_{N,N}, V_{N,N})$ be their deformed coordinates in $\mathcal{D}_2$. Let also $\mathcal{I}_{i,j}$ be an indicator function defined for each pixel in $\mathcal{D}_1$ such that $\mathcal{I}_{i,j}$ is unity when the point $(x_{i,j}, y_{i,j})$ has a point of correspondence, say $(f^U_{i,j}, f^V_{i,j})$, in $\mathcal{D}_2$ and is zero otherwise. Points of correspondence in $\mathcal{D}_1$ are given by $\mathbf{x}^k_0, \ldots, \mathbf{x}^k_M$, $k = 1, \ldots, K$, together with any manually provided landmarks. We then define the points $(U_{0,0}, V_{0,0})$ through $(U_{N,N}, V_{N,N})$ to be those that jointly minimize

$$E = \lambda E_E + E_F \,, \tag{7}$$

where

$$E_E = \sum_{i=0}^{N-1}\sum_{j=0}^{N-1} \left[(U_{i+1,j} - U_{i,j})^2 + (U_{i,j+1} - U_{i,j})^2 + (V_{i+1,j} - V_{i,j})^2 + (V_{i,j+1} - V_{i,j})^2\right] , \tag{8}$$

$$E_F = \sum_{i=1}^{N-1}\sum_{j=1}^{N-1} \left[\mathcal{I}_{i,j}\left((U_{i,j} - f^U_{i,j})^2 + (V_{i,j} - f^V_{i,j})^2\right)\right] \tag{9}$$

subject to the boundary conditions

$$\begin{aligned} (U_{0,i}, V_{0,i}) &= (a, i) \quad , \quad (U_{N,i}, V_{N,i}) = (b, i) \,, \\ (U_{i,0}, V_{0,i}) &= (i, c) \quad , \quad (U_{i,N}, V_{i,N}) = (i, d) \,, \end{aligned} \tag{10}$$

for $i = 0, \ldots, N$. The boundary conditions set the coordinates of the transformed image frame. The four constants a, b, c, d are chosen so that the distance of the outer cortex from the boundaries of $\mathcal{D}_1$ and $\mathcal{D}_2$ is the same for both images. They are determined automatically from the outer cortical contours.

By taking derivatives of (7) one can show the necessary conditions

$$\begin{aligned} \lambda(4U_{i,j} - U_{i+1,j} - U_{i-1,j} - U_{i,j+1} - U_{i,j-1}) + I_{i,j}(U_{i,j} - f^U_{i,j}) &= 0 \,, \\ \lambda(4V_{i,j} - V_{i+1,j} - V_{i-1,j} - V_{i,j+1} - V_{i,j-1}) + I_{i,j}(V_{i,j} - f^V_{i,j}) &= 0 \,, \end{aligned} \tag{11}$$

which must be satisfied for $1 \geq i, j \geq N-1$. These equations give a force balance condition which is satisfied by a dynamic system in equilibrium — i.e., the sum of the forces exerted on each deformed pixel must be zero. We solve Equations (11) iteratively using the Gauss-Seidel method.

There is a certain similarity between the EDT transformation and the spline interpolation approach proposed by Bookstein in [17]. There are two key differences, however. First, EDT does not force an absolute matching of the landmark points as in [17]. Instead, it merely penalizes deformations that do not maintain the specified correspondence. This difference is important when the location of the landmarks are in error, a condition that can be expected to some degree from our active contour algorithm. Second, EDT is formulated as a boundary-value problem rather than an interpolation problem as in [17]. Boundary-value problems eliminate the large fluctuations one may see when far from the landmark points using spline interpolation methods.

IV. Experimental Results

In this section we demonstrate the performance of our registration approach using three different data sets.

1. Baboon Images.

Fig. 3 shows two images of approximately the same mid-brain coronal section of a baboon brain, to which a stroke was introduced. Fig 3b shows a T_1-weighted magnetic resonance image, while Fig. 3a shows a photographic image taken after the animal was sacrificed and its brain was dissected. Registration of these images allows post-mortem analysis of the tissue at the stroke area to be correlated to the MR image.

Although the images in Figs. 3a and 3b represent the same coronal cross-section (to good approximation), several gross morphological differences between the two are apparent. First, the overall shape of the brain is different. In particular, the post-mortem image is squashed vertically. This effect is largely the result of gravity acting on the brain during fixation. Second, the sulci are more pronounced in the post-mortem photograph. This is the result of brain matter shrinkage, again due to the fixing process. Third, there is a tear in the gray matter at the upper right of the post-mortem image caused by the cutting procedure. Finally, the temporal lobes are pushed farther apart from the brain stem in comparison to the MR image. This again is due to the settling that occurred during fixation. These differences are highlighted in Fig. 3b, which overlays the boundary of the cortex in Fig. 3a onto the MR image.

We next applied the active contour algorithm described in Section III to the images in Fig. 3. In both cases a histogram-based region growing algorithm was used to segment the parenchyma (white and grey matter). A separate threshold and one seed point was selected manually for each image. After determining the parenchyma, two landmark points per image, sitting on the temporal lobes, were designated manually as the endpoints of each active contour. The remaining points on the active contour were initialized to the rectangular im-

age frames, and the active contour algorithm was run to convergence.

The final active contours are shown in Fig. 4 superposed as a sequence of white dots on the original images. To give a visual indication of how well the active contour algorithm provided point correspondence, in Fig. 5 we highlighted some key points on the post-mortem image and their corresponding points on the MR image. We note that the points on the left and right Sylvian fissures, the points on the left and right superior temporal sulci, and the points on the superior frontal gyri near the midline are very close to where one would manually place them. This confirms that the isometric transformation of the active contours provides good landmark points, automatically.

We next applied EDT using the active contours shown in Fig. 4. The result is shown in Fig. 6, where Fig. 6a shows the transformed post-mortem image and Fig. 6b shows the cortical outline of the transformed image superposed on the MR image. The superposed cortical outline shown in Fig. 6b is extremely close to the MR outline at all regions including the temporal lobes. Visual comparison of Fig. 6a with the original MR image (e.g., Fig. 3b or the underlying image in Fig.6b) shows that the shapes of many of the cortical gyrations are now quite similar to each other.

2. Registration of atlas and MR images.

This experiment demonstrates the registration of two different brains imaged with two different modalities. The first image, shown in Fig. 7a, is an atlas image showing the human brain cortex within the left hemisphere of a horizontal (relative to the AC-PC line) brain section. The atlas image corresponds to Fig. 119 in [18]. The second image, shown in Fig. 7b, is an MR image of the corresponding cross-section of a patient brain. This image pair presents a problem for all similarity-based image registration methods since there is no model for how the brightness of one image is related to the other. The problem must be solved using either landmark point methods or boundary methods. Our approach provides a flavor of both approaches with significant automation.

Using the frontal and occipital poles as endpoints, we applied our active contour algorithm to each image in Fig. 7. EDT was applied using the cortical contours as landmark points. The transformed atlas image is shown in Fig. 7c, and its outline is shown in Fig. 7d superposed on the original MR image. We see that a good registration of the general shape of the cortical contours was obtained. The registration error for this data set, however, is larger than that of the baboon data. We must expect this to some extent since these images represent different brains.

3. Ventricular Registration.

For our final experiment we considered a set of three images obtained from human subjects with enlarged ventricles (Figs. 8a–c). Each of these images was obtained at the same orientation and level of the brain, and approximately at the same orientation and level of the atlas image shown in Fig. 8d. In these images, because of the large differences in the size and shape of the ventricles, we used three curves in the registration process: the cortical boundary, and the upper and lower ventricular boundaries. These three boundaries, obtained through three region growing procedures for each patient image, are shown in Fig. 9 superimposed on the atlas image. Fig. 9 reveals a large misregistration, despite the similarity in the acquisition procedure of these images.

After mapping the three types of curves mentioned above of each of the patient images onto their counterparts of the atlas image, we selected 15 of the resulting 1067 points of correspondence determined automatically through the active contour algorithm. These points are shown in Fig. 10 for the three MR images and the atlas image. Figure 10 reveals a good correspondence.

We then applied EDT, mapping the atlas image onto each of the patient images. The resulting warped atlas image for each patient image is shown in Fig. 11 superimposed on the same boundaries as the ones in Fig. 9. From Fig. 11 we see that the atlas image was adapted to the shape of each patient image yielding a good registration.

V. CONCLUSION

We have presented a new two-step approach for brain image registration which accounts for highly nonlinear deformations. In the first step we obtain a one-to-one mapping between a set of curves that can be identified in the two brain images, using an active contour algorithm. This step establishes the correspondence of a large number of points with minimal human intervention. The second step transforms the coordinate space of one image to the other using these points of correspondence. An elastic transformation — EDT — was proposed. This transformation modeled the images as elastic sheets that deform under a set of external forces defined on the curves for which a mapping was obtained in the first step of the algorithm.

The overall approach was verified qualitatively using three cases: a post-mortem photograph and MRI pair, and two atlas and MRI registration problems. In the first pair, our active contour algorithm was shown to provide a good estimate of the outer cortical boundaries with superb point-to-point correspondence. The only manual intervention required was the specification of two seed points for region growing and four endpoints for the active contours. In the second stage of the registration procedure, EDT provided excellent maps of the cortical boundaries and of the brain interior. In the second and third image pairs (MRI and atlas) we demonstrated a good matching using EDT. A remarkably good matching was obtained in the third experiment, despite the highly nonlinear deformation that was present in the ventricular area.

Improvement in the performance of the active contour algorithm might be obtained by incorporating landmark points through the concept of control points [16, 1]. In this technique, specific points on the outer cortex would attract specific points on each active contour through additional external forces. This could improve point correspondence of the entire active contour if large errors are otherwise observed.

Extension of this approach to three dimensions is also possible through the use of active surfaces [19] instead of active contours. Since it is generally not possible to achieve an isometric mapping of two surfaces, we cannot expect the landmark points generated by an active surface to be as good as those generated by an active contour. Therefore, methods that force landmark point matching, such as Bookstein's approach, may not be a wise choice for step two. In contrast, because it does not force landmark points to match and it is readily extensible to three dimensions, EDT appears to be a good option for a three-dimensional transformation using active surface pairs.

Acknowledgements

This work was supported in part by the grant "Developmental Pathways to Learning Disabilities" (NICHD P50HD 25806-03) and by National Science Foundation grant MIP-9350336.

References

[1] C.A. Davatzikos and J.L. Prince. An active contour model for mapping the cortex. Technical Report JHU/ECE 93-06, Johns Hopkins University, 1993. Submitted to the IEEE Transactions on Medical Imaging.

[2] J.C. Mazziotta, C.C. Pelizzari, G.T. Chen, F.L. Bookstein, and D. Valentino. Region of interest issues: The relationship between structure and function in the brain. *Journal of Cerebral Blood Flow and Metabolism*, pages A51–A56, 1991.

[3] M.Singh, R.R. Brechner, and V.W. Henderson. Neuromagnetic localization using magnetic resonance images. *IEEE Transactions on Medical Imaging*, 11(1):129–134, 1992.

[4] A.C. Evans, W. Dai, L. Collins, P. Neeling, and S. Marett. Warping of a computerized 3-d atlas to match brain image volumes for quantitative neuroanatomical and functional analysis. *Proc. of the SPIE conf. on Image Processing*, 1445:236–246, 1991.

[5] Y.S. Abu-Mostafa and D. Psaltis. Image normalization by complex moments. *IEEE Transactions on Pattern Analysis and Machine Intelligence*, 7(1):46–55, 1985.

[6] F.L. Bookstein. Thin-plate splines and the atlas problem for biomedical images. *Proc. of the 12th Int. Conf. on Information processing in medical imaginig*, pages 326–342, 1991.

[7] Chaim Broit. *Optimal Registration of Deformed Images*. PhD thesis, University of Pennsylvania, 1981.

[8] R. Bajcsy, R. Lieberson, and M. Reivich. A computerized system for the elastic matching of deformed radiographic images to idealized atlas images. *Journal of Computer Assisted Tomography*, 7(4):618–625, 1983.

[9] G.E. Christenesen, R.D. Rabitt, and M.I. Miller. A deformable neuroanatomy textbook based on viscous fluid mechanics. *Proc. of 27th Annual Conference on Information Sciences and Systems*, pages 211–216, 1993.

[10] Mehran Moshfegi. Elastic matching of multimodality medical images. *CVGIP:Graphical Models and Image Processing*, 53(3):271–282, 1991.

[11] C.A. Pelizzari, G.T.Y Chen, D.R Spelbring, R.R. Weichselbaum, and C.T. Chen. Accurate three-dimensional registration of ct, pet, and/or mr images of the brain. *Journal of Computer Assisted Tomography*, 13(1):20–26, 1989.

[12] J.P. Thirion, O. Monga, S. Benayoun, A. Gueziec, and N. Ayache. Automatic registration of 3-d images using surface curvature. *Proc. of the SPIE Conf. on Mathematical methods in medical imaging*, 1768:206–216, 1992.

[13] C.A. Davatzikos and J. Prince. Segmentation and mapping of highly convoluted contours with applications to medical images. *Proc. of ICASSP'92, IEEE Conf. on Acoust., Speech and Signal Proc.*, 1992.

[14] C.A. Davatzikos and J.L. Prince. Convergence analysis of the active contour model with applications to medical images. *SPIE proc.— Visual Communications and Image Processing*, 1992.

[15] C.A. Davatzikos and J.L. Prince. Adaptive active contour algorithms for extracting and mapping thick curves. *Proc. of the IEEE Comp. Vision and Patt. Recognition Conference, CVPR'93*, pages 524–529, 1993.

[16] M. Kass, A. Witkin, and D. Terzopoulos. Snakes: Active contour models. *International Journal of Computer Vision*, 1:321–331, 1988.

[17] F.L. Bookstein. Principal warps: Thin-plate splines and the decomposition of deformations. *IEEE Transactions on Pattern Analysis and Machine Intelligence*, pages 567–585, 1989.

[18] J. Talairach and P. Tournoux. *Co-planar stereotaxic atlas of the human brain*. Thieme, 1988.

[19] Isaac Cohen, Laurent D. Cohen, and Nicholas Ayache. Using deformable surfaces to segment 3-D images and infer differential structures. *CVGIP: Image Understanding*, September 1992.

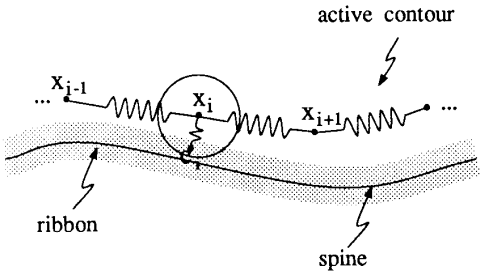

Figure 1. A mechanical analog of the active contour.

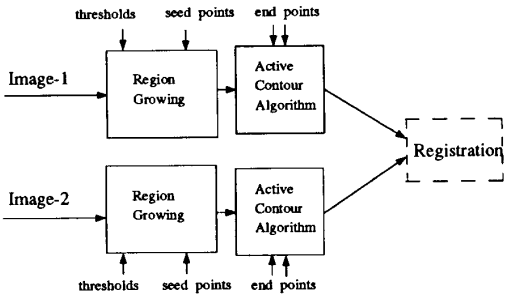

Figure 2. A block diagram of the approach proposed in this paper.

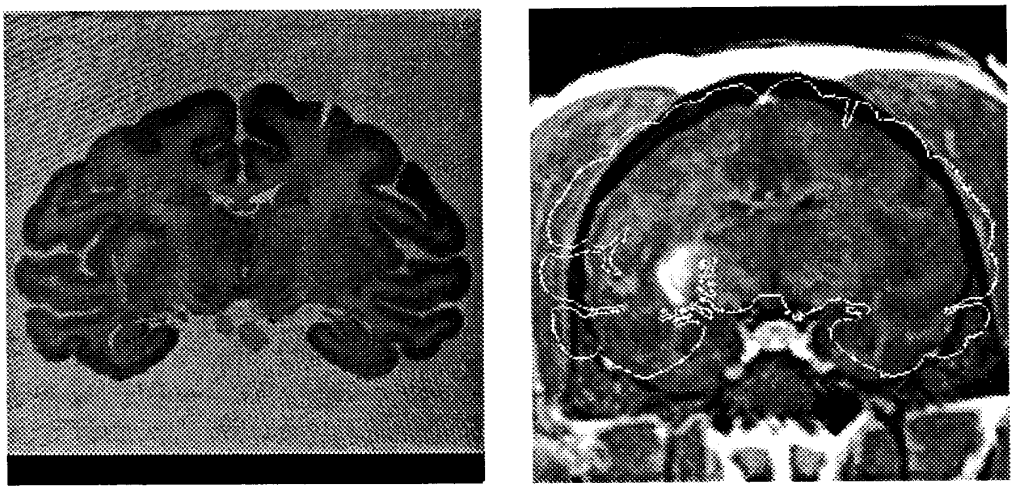

(a) (b)

Figure 3. (a) A post-mortem photograph of a baboon brain cross-section. (b) An MR image of the same, approximately, cross-section superimposed on the outline of (a).

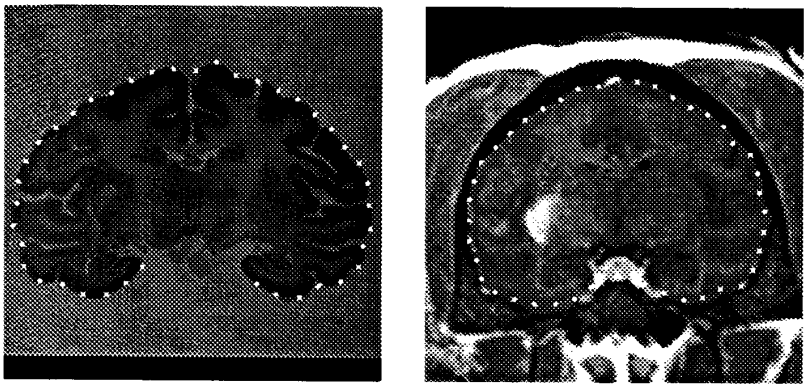

(a) (b)

Figure 4. The cortical outline obtained through the active contour algorithm for (a) the image of Fig. 3a and (b) the image of Fig. 3b.

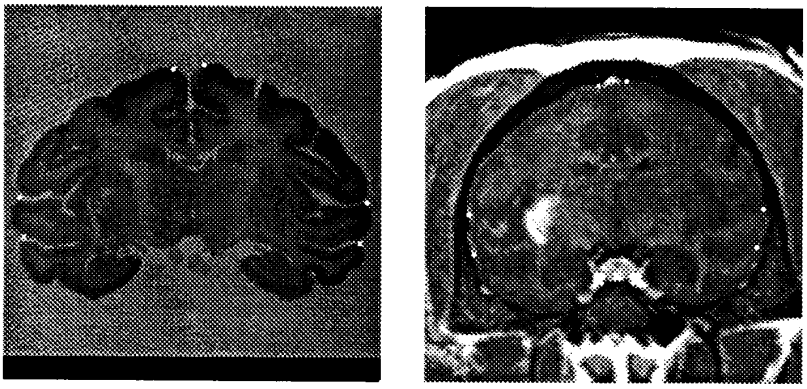

(a) (b)

Figure 5. Demonstration of the automatic landmark-point generation through the active contour algorithm: (a) six selected active contour points of the active contour configuration shown in Fig. 4a and (b) their corresponding points of the active contour configuration shown in Fig. 4b.

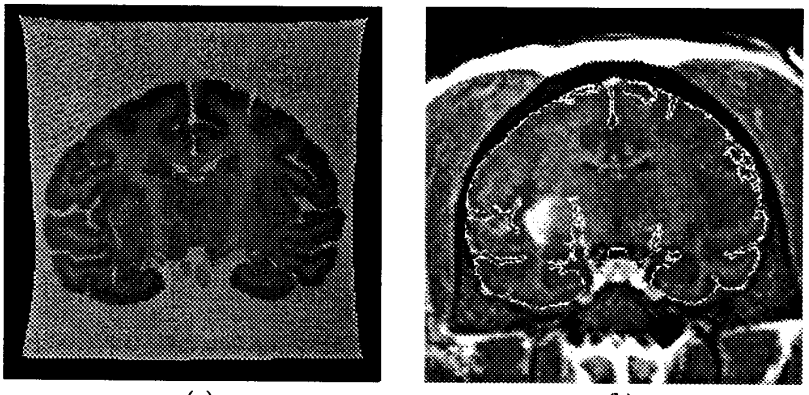

(a) (b)

Figure 6. (a) The image of Fig. 3a transformed using EDT and (b) the cortical outline of (a) superimposed on the MR image.

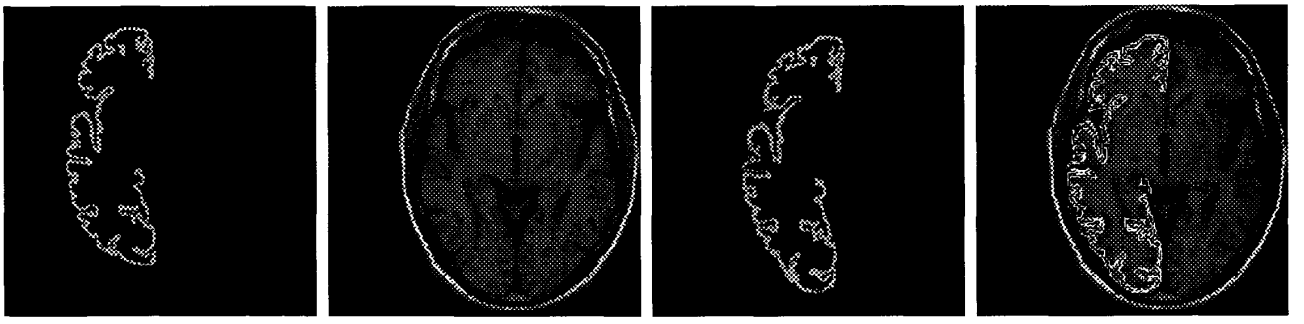

(a) (b) (c) (d)

Figure 7. (a) A Talairach atlas image of the human brain, (b) an MR transaxial image of the corresponding cross-section, (c) the atlas image transformed using EDT, and (d) the cortical outline of (c) superimposed on (b).

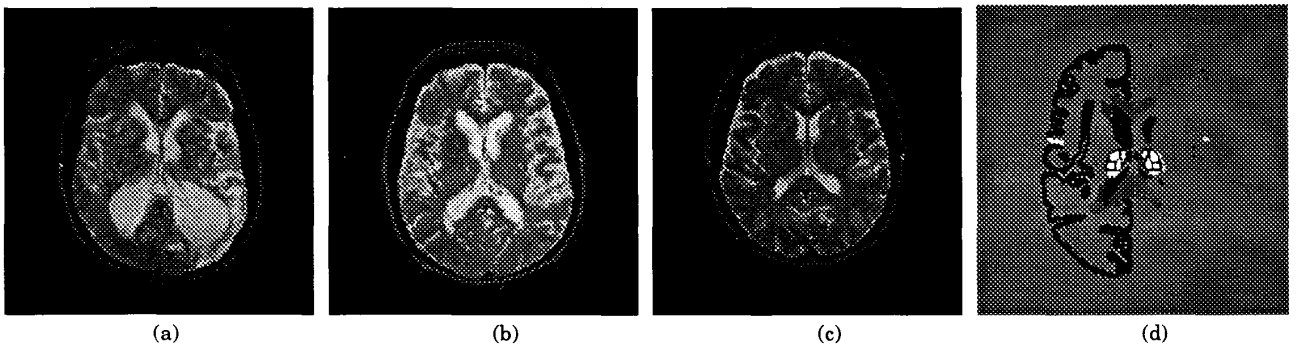

(a) (b) (c) (d)

Figure 8: (a)–(c) Three MR images obtained from patients with enlarged ventricles and (d) a Talairach atlas image obtained from the same, approximately, level of the brain.

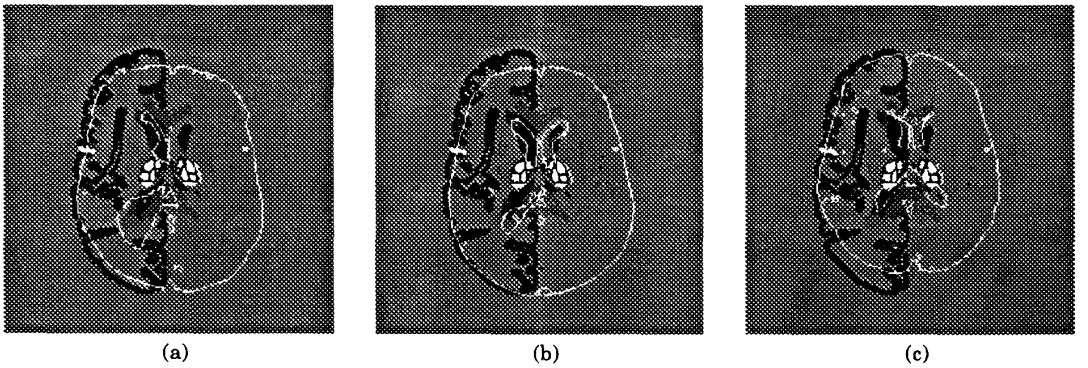

(a) (b) (c)

Figure 9: The cortical and ventricular outlines of Figures 8a–8c superimposed on Fig. 8d. The mismatch is apparent.

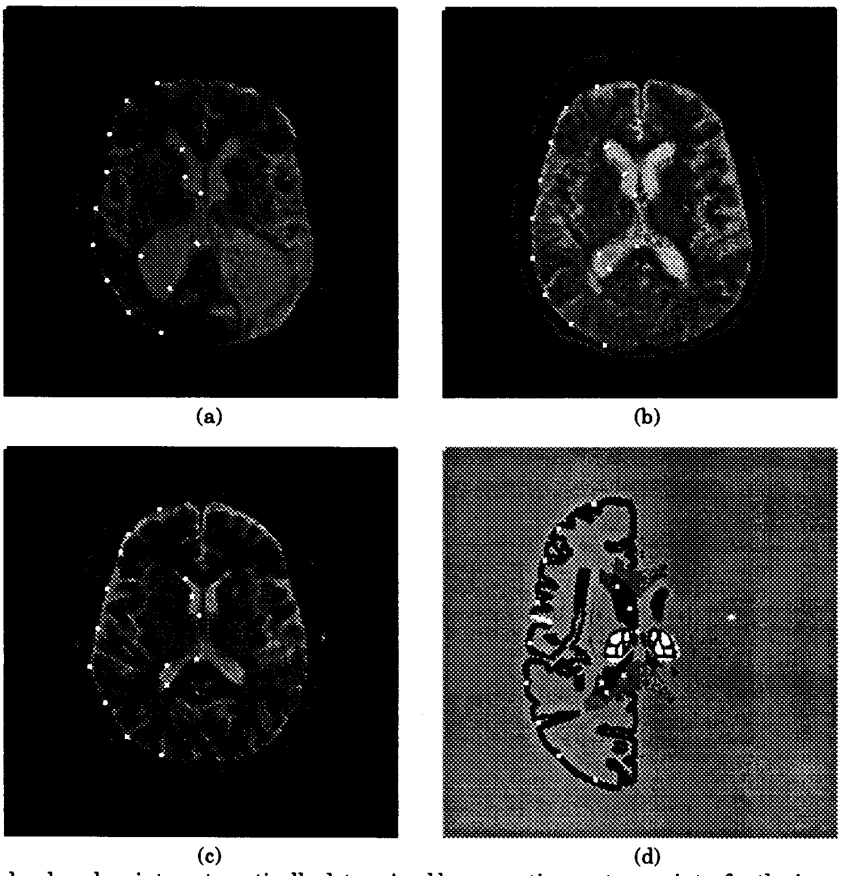

Figure 10. The landmark points automatically determined by our active contour points, for the images of Fig. 8.

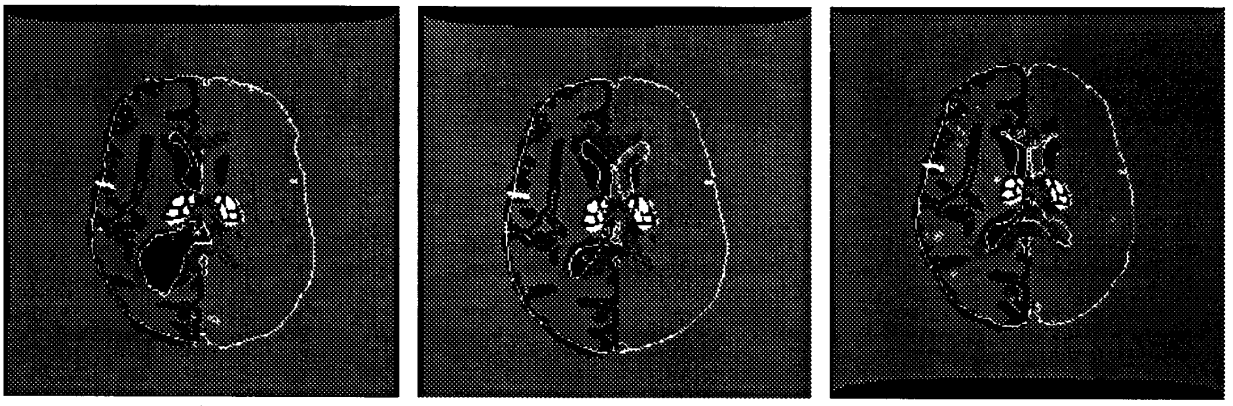

Figure 11: The warped atlas image of Fig. 8g superimposed on the cortical and ventricular outlines of the images of Figs. 8a–8c. A good registration of the cortical and the ventricular area was obtained.